

Chapter 2

High Strain Rate Performance of Pressureless Sintered Boron Carbide

Tomoko Sano, Matthew Shaeffer, Lionel Vargas-Gonzalez, and Joshua Pomerantz

Abstract The processing technique used to consolidate ceramics powders can have a large effect on the microstructure, and hence the performance of the material. In this research, microstructure, mechanical properties, and the high strain rate compressive behavior of pressureless sintered boron carbide (B_4C) samples were examined and compared to those of conventional hot pressed B_4C . Penetration velocity tests were conducted on identical targets made with the pressureless sintered B_4C samples and hot pressed B_4C . Microstructural and post mortem characterization showed that test results of the pressureless sintered B_4C were affected by significant porosity in the samples. The effects of the processing technique on the microstructure, properties, and the high rate behavior of the pressureless sintered B_4C will be discussed.

Keywords Boron carbide • Pressureless sintering • Microstructure • High rate behavior

2.1 Introduction

Boron Carbide (B_4C) is used widely in abrasive, wear resistant components, and armor applications due to its high hardness and low density properties. Hot pressing B_4C powder is the typical commercial technique used to form personnel armor plates and components for various applications. B_4C components can reach nearly full theoretical density by the hot pressing technique, which requires vacuum or inert atmosphere, sintering temperatures near 2,300 K, and pressures up to 40 MPa [1]. The hot pressing technique using additives allows densification at lower temperatures, improves oxidation and thermal shock resistance, and increases mechanical properties by inhibiting grain growth. The limitation of the hot pressing technique is the high operation cost per batch and only plates or cylindrical shapes of a limited size can be produced. Also, in addition to a larger die, to achieve the same pressure applied to a smaller specimen, a much larger hot press equipment size is required for larger specimens. Another technique, pressureless sintering, is also used to consolidate and densify B_4C powders [2–4]. The pressureless sintering technique is a less expensive method, but requires fine grained starting power ($<3\ \mu m$), higher temperatures (roughly 2,500 K) and amorphous carbon additions to achieve greater than 95 % theoretical density [5]. In both techniques, the additives could form precipitates or secondary phases at the grain boundaries that are detrimental to the mechanical performance.

In addition to quasi-static behavior, high rate compressive behavior is often tested using the Kolsky bar to evaluate the failure of structural ceramic materials [6, 7]. The high strain rate compressive behavior of B_4C has been studied by Paliwal and Ramesh [8]. In their experiment using the Kolsky bar, they determined at strain rates between 10^2 and $10^4/s$, the peak compressive strength of a hot pressed B_4C sample reached 3.8 GPa. A similar study [9] on high strain rate compression testing also using the Kolsky bar comparing the baseline hot pressed B_4C results from Paliwal and Ramesh to two types of pressureless sintered B_4C , one hot isostatically pressed (HIPed) and the other sintered. All three B_4C types showed

T. Sano (✉) • L. Vargas-Gonzalez • J. Pomerantz
U.S. Army Research Laboratory, 4600 Deer Creek Loop, Aberdeen Proving Ground, MD 21005, USA
e-mail: tomoko.sano.civ@mail.mil

M. Shaeffer
Johns Hopkins University, Center for Advanced Metallic and Ceramic Systems, 028 Latrobe Hall, 3400 N. Charles St.,
Baltimore, MD 21218, USA

comparable compressive strengths. The HIPed samples' compressive strength distribution ranged from 3.4 to 4.0 GPa, falling within the 3.1–4 GPa range of the hot pressed samples, and the sintered samples ranged from just over 3.0–3.7 GPa.

An often applied technique to evaluate the penetration resistance of armor materials is by the V_{50} test [10]. Several B_4C samples have been tested in the past, with various target assembly. One such impact test [11] which compared the V_{50} technique to depth of penetration measurements, tested 6 in. B_4C tiles (presumed to be hot pressed) with thicknesses of 1.0, 1.5, and 2.0 in. The B_4C was observed to have performed better compared to similarly tested silicon carbide (SiC) and 90 % alumina (Al_2O_3). A recent work by Dateraksa et al. [12] determined the V_{50} values of $100 \times 100 \text{ mm}^2$ Al_2O_3 , SiC and hot pressed B_4C tiles with S2 – glass composite backing plates. The V_{50} of the hot pressed B_4C was determined to be 829 m/s, or 2,720 ft/s and had the lowest V_{50} value of the materials tested.

2.2 Experimental

Pressureless sintered square B_4C tiles with the nominal dimensions of $50 \times 50 \times 8 \text{ mm}$, and hexagonal tiles with the nominal dimensions of 35 mm flat to flat and 20 mm thick were obtained. Density was measured by the Archimedes principle for both tile morphologies. For microstructural characterization and hardness measurements, samples from each tile morphology were cut, mounted with a Buehler cold mount epoxy, and polished on the Struers Rotopol-31 with decreasing diamond suspension sizes starting with 45 μm and ending with 0.25 μm . Microstructural and elemental characterizations were conducted on the FEI Nova NanoSEM600 (FEI Company, Hillsboro, OR) scanning electron microscope (SEM), and EDAX Pegasus XM4 (EDAX Inc. Mahwah, NJ) energy dispersive spectroscopy (EDS), respectively. X-ray diffraction spectra were obtained with the Siemens 05005 diffractometer for phase analysis. The polished samples were subjected to Knoop microindentation (Wilson Tukon 2100, Wilson Hardness, Norwood, MA) at 1.0, 2.9, 4.9, 9.8, and 24.5 Newton loads.

From the square tiles, flexural specimens according to the ASTM C1161 type B standard [13], and high strain rate compression samples with cuboidal dimensions $3.5 \times 4.0 \times 5.3 \text{ mm}$ were machined by Bomas Machine Specialties Inc., Somerville, MA. Two sets of samples were machined such that for one set of samples, the loading surface ($3.5 \times 4.0 \text{ mm}$) was parallel to the square surface (referred to as “horizontal samples”) and the other set of samples, the loading surface was perpendicular to the square surface (referred to as “vertical samples”). A set of horizontal and a set of vertical compression samples were also machined from the hexagonal tile with the same dimensions. Flexural strength experiments were conducted on the Instron 5500R load frame (Instron, Norwood, MA) with a lower support span of $L = 40 \text{ mm}$ and an upper support span of $U = 20 \text{ mm}$. The width and thickness of the flexural specimens were recorded and loaded at 0.5 mm/min. Tests were conducted according to ASTM C1161.

High strain rate compression testing on the Kolsky bar with the same test setup as Paliwal and Ramesh [8] was conducted on five compression specimens from each sample set (square plate horizontal, vertical, hexagonal plate horizontal and vertical). Before testing, each specimen was measured for variance in the angle of the corners and the parallelism. A high speed camera was used to capture the specimen failure at 2.4 microsecond intervals with exposure times ranging from 230 nanoseconds to 1 microsecond, and the post mortem fragments were collected in a plexiglass box surrounding the specimen for SEM characterization.

To assess the penetration resistance of the pressureless sintered B_4C material, ceramic/ultra-high molecular weight polyethylene (UHMWPE) composite specimens were manufactured. Ten $50.8 \times 50.8 \times 07.4 \text{ mm}$ samples were supplied for testing. A commercially available hot-pressed B_4C material (PAD – B_4C , CoorsTek, Inc. Vista, Vista, CA) was also procured at the same size to serve as the performance baseline. The composite backings were manufactured using Spectra Shield II® SR-3136 (Honeywell Specialty Materials, Morristown, NJ), a UHMWPE fiber and thermoplastic matrix sheet product. Each tile was bonded to the center of each composite backing using Sikaflex-252, a moisture-cure polyurethane-based sealant. Small strips of a 0.5 mm nylon line were used to control the adhesive thickness. The composite specimens were placed underneath a vacuum bag and cured under vacuum for 1 week at ambient room temperature.

The penetration resistance of the composite panels was evaluated through tests which are used to experimentally determine the probabilistic limit velocity (V_{50}) and derive a probabilistic curve. The probabilistic V_{50} value corresponds to the velocity at which the probability of the projectile being stopped or the projectile penetrating through the panel is at 50 %. The testing and the determination of the V_{50} value was conducted as specified in the MIL-STD-662F standard [10]. Each panel was impacted in the center of the ceramic strike face with a test projectile fired from a universal receiver. Impact velocities are varied until there are several partial and complete penetration values within a specified range of velocities. The values within the range of velocities are average to determine the V_{50} result. If a mixed mode of values within the specified range is obtained, then the entire range of tests can be input into a calculation algorithm to generate a logistic regression

curve. The mixed mode of results is a case in which the highest measured partial penetration velocities are slightly higher than the lowest complete penetration velocities. The logistic regression curve provides calculated probabilities of resistance to penetration of the composite panels throughout an entire V_0 to V_{100} range (V_0 being the velocity at which no projectiles will penetrate to V_{100} where all projectiles will penetrate).

2.3 Results and Discussion

For the square tiles, the density was measured to be 2.40 g/cm^3 or 95 % theoretical density, and 2.38 g/cm^3 or 94 % theoretical density for the hexagonal tiles. The porosity and graphite particles are believed to be the reason for less than full density. Microstructural and elemental characterization in the SEM was conducted on both square and hexagonal tiles samples. Numerous graphite particles (black areas) and some twinned grains were observed. Figure 2.1 shows the SEM micrograph of the hexagonal tile microstructure and that of PAD – B_4C . The EDS spectra collected showed 78 atomic % B, 22 atomic % C. XRD spectra were obtained for both the square plate and hexagonal plates. An example of the spectra from a hexagonal sample is shown in Fig. 2.2.

Ten Knoop indents were measured at each load for polished samples from the square and hexagonal tiles according to ASTM standard C1326 [14]. The average hardness (HK) at 24.5 N will be reported, as recommended by ASTM C1326 and by Swab [15]. At loads equal to or higher than 19.6 N, B_4C is load independent, and unaffected by the indentation size effect. For the square tile the HK was calculated to be 19.8 GPa with a standard deviation of 1.2 GPa. For the hexagonal tile, the HK was 20.1 GPa with a standard deviation of 1.6 GPa. These results are tabulated in Table 2.1, with the properties of the baseline hot pressed PAD – B_4C (from formerly BAE Systems, now CoorsTek). Although the HK values of the square and

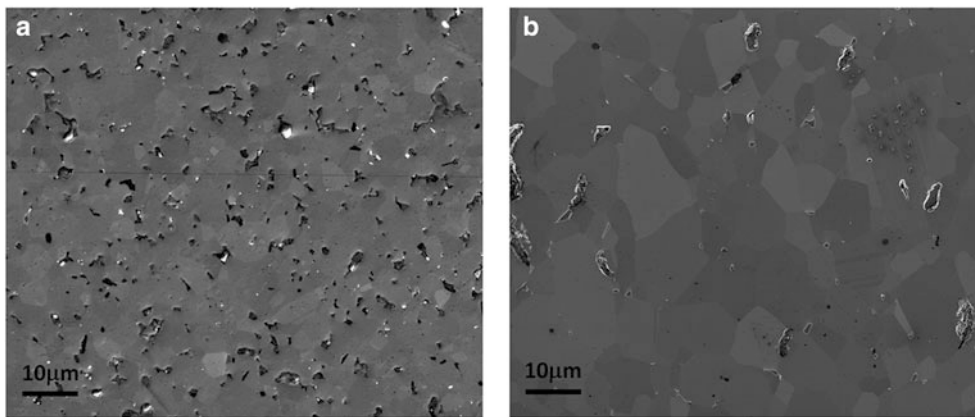


Fig. 2.1 SEM micrographs of the polished surface of (a) the hexagonal tile and (b) PAD – B_4C

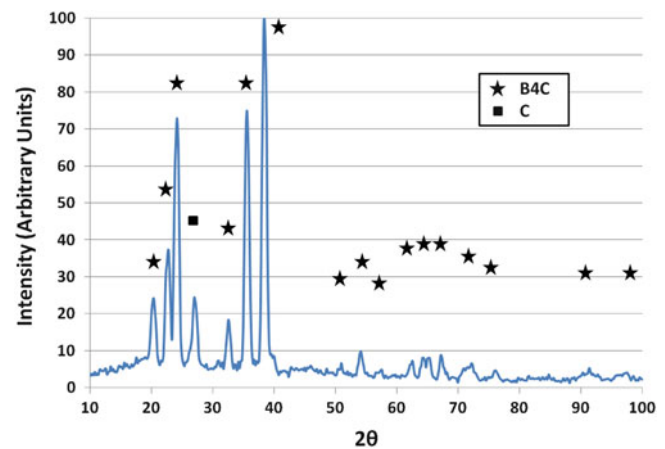
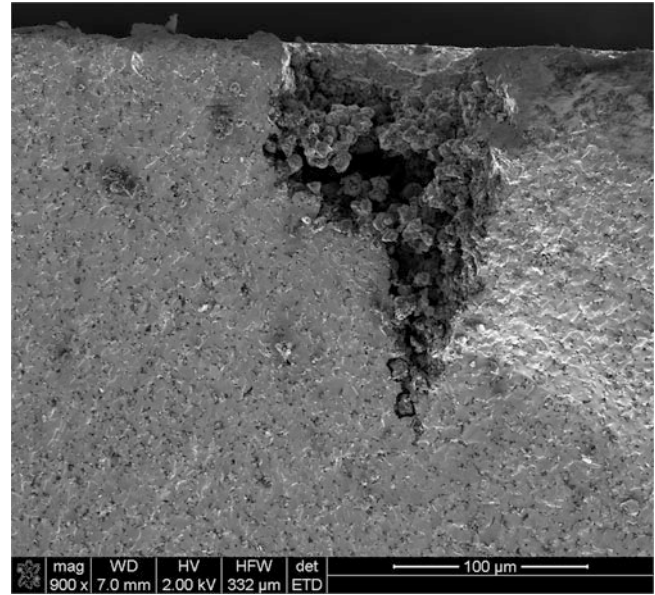


Fig. 2.2 XRD spectra of the hexagonal sample

Table 2.1 B₄C properties

	Density (g/cm ³)	HK (GPa)	Flexural strength (MPa)
Square plate	2.40	19.8	295 ± 38
Hexagonal plate	2.38	20.1	–
PAD [16]	2.50	19.9 (HK2)	398 ± 34

Fig. 2.3 A large pore observed in the fracture surface of the bar with the lowest flexural strength



hexagonal plates are comparable to the PAD – B₄C, several indents could not be measured due to the indents landing on a pore on the surface or just under the surface, causing severe cracking around the indent.

Four point flexure testing was conducted on 52 type B bars from the square tiles to determine the average flexural strength. The flexural strength was calculated using the following equation,

$$S = \frac{3PL}{4BD^2} \quad (2.1)$$

where S is the flexural strength, P is the break force, L is the outer support span, B is the width, and D is the thickness. The average flexural strength was 295 MPa with a standard deviation of 38 MPa at an average break force of 355 MPa. This value as well as that of PAD – B₄C are listed in Table 2.1. Fractography was conducted on the bar with the highest flexural strength of 366 MPa, and the bar with the lowest flexural strength of 212 MPa. Both bars failed by brittle transgranular fracture and revealed numerous porosities. Just like porosity was a factor in the hardness measurements, porosity significantly affected flexural strength. The bar with the lowest flexural strength had a significant pore, or a region of poor consolidation, shown in Fig. 2.3, where the fracture initiated.

High rate compression experiments were conducted on five samples from each of the plate types, and compared to the results of the baseline PAD – B₄C [8, 9]. The compressive strengths averages ranged from 2.9 to 3.7 GPa. A plot comparing the compressive strengths is shown in Fig. 2.4. Besides the hexagonal plate horizontal sample set showing a decreased compressive strength, the pressureless sintered plates preformed comparably to the PAD – B₄C. The outlier point at 1.3 GPa in the square plate, horizontal direction is believed to be a porous or sample with other significant flaws. Images captured by the high speed camera of this sample show a surface crack propagating across the length of the sample even before experiencing 0.5 GPa of stress. Images from tests on other samples also show surface cracks propagating across the samples, but at stresses much closer to the maximum observed stresses, as shown in Fig. 2.5. Figure 2.5 is the stress and strain versus time for a hexagonal sample in the horizontal direction that achieved 3.17 GPa compressive strength. The numbers along the stress curve indicate when the accompanying high speed camera images were captured. In Fig. 2.5b, image 5 captured at the maximum stress, the sample is still intact, showing only surface cracks at the strike face and the front corners. It is not until image 6, after reaching the peak stress when the volumetric strain starts to increase, does the sample show significant failure

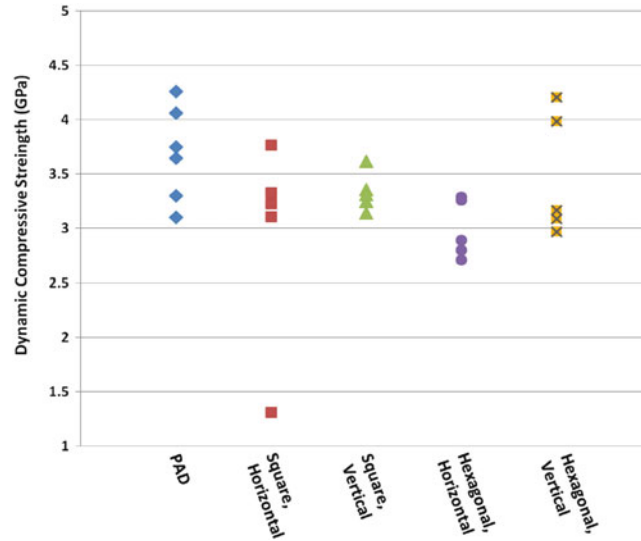


Fig. 2.4 Compressive strength of baseline PAD B4C, square, and hexagonal plates

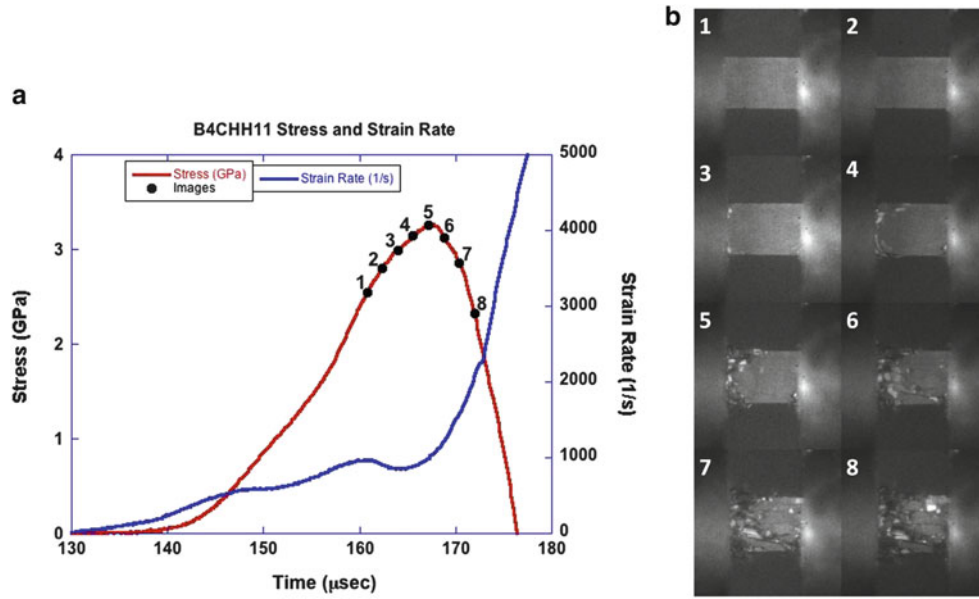
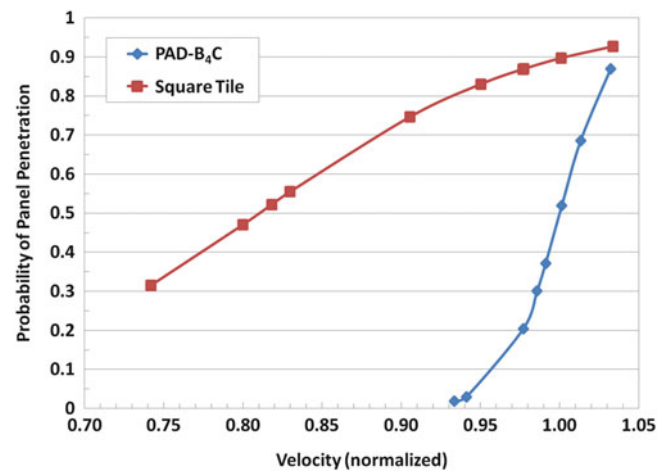


Fig. 2.5 (a) Plot of stress and strain versus time for the high strain rate compression testing of a hexagonal sample in the horizontal direction, and (b) high speed camera images of the sample during the experiment, captured at the numbered points along the stress curve

and surface cracks propagating across the length of the sample. This behavior has been observed in other ceramics [6] including SiC and Al₂O₃.

Fragments collected from the high strain rate compression experiments were evaluated in the SEM. No noticeable distinction was observed between the samples that performing better and those that performed poorly. All sample fragments showed evidence of transgranular fracture. Visual inspection of the collected fragments from all tests gave no quantitative indication whether the set of fragments were from a sample with higher or lower compressive strength. Several researchers [17–21] have correlated the average fragment size and size distribution to the defect density and strain rate at high loading rates. It has been observed that higher strain rate loading results in smaller fragment sizes and narrower fragment size distribution [20, 21] and that fracture stress scales with strain rate to the 1/3 power [18]. In this present study, the strain rates were comparable for all Kolsky bar experiments, so this observation cannot be confirmed. Although Keller and Zhou [22] found no correlation between fragments size distributions, average fragment size and material strength of TiB₂-Al₂O₃

Fig. 2.6 Probability of panel penetration versus normalized impact velocity



ceramics, Moynihan et al. determined [23] that there is a link between fragmentation (and resulting fragment size distribution) to the failure mechanisms and the ballistic performance for B₄C. More samples of PAD, square, and hexagonal tiles need to be tested at a range of strain rates to correlate the fragment size and size distribution to the compressive strength.

The penetration tests were conducted at the same range in the same conditions for the PAD – B₄C and square plate B₄C samples. The V_{50} values for the PAD-B₄C and square tile B₄C panels were normalized with respect to the PAD-B₄C value (value of 1.00 with a standard deviation of 0.016). The square tile B₄C panels performed considerably worse than the PAD-B₄C panels, with a normalized V_{50} value of 0.810 with a large standard deviation of 0.082. Figure 2.6 shows the probability of panel penetration at various normalized impact velocities. The significance of the difference in performance is evident when you compare the panels near the normalized value of 0.94; PAD-B₄C has a 3 % probability while the square tile panel has over 80 % probability of panel penetration. If the probability curve is extrapolated based on the current data trend, the data would asymptotically curve toward a V_0 near the normalized penetration value of 0.60–0.65 (compared to the calculated V_0 value of PAD-B₄C near 0.92–0.93).

2.4 Conclusions

The microstructure, mechanical properties, and impact properties of pressureless sintered B₄C in two tile shapes were evaluated. The results were compared with baseline PAD – B₄C to determine the effects of the pressureless sintering on the various properties. It was determined that the porosity due to inadequate consolidation and sintering in the pressureless sintered tiles adversely affected the density, flexural strength, and the penetration values. However the pressureless sintered samples had no impurities, and showed comparable hardness and high strain rate compressive strength. It is believed that with reduced porosity, the mechanical properties and penetration properties of the pressureless sintered B₄C would be comparable to those of PAD-B₄C.

References

1. Thévenot F (1990) Boron carbide – a comprehensive review. *J Eur Ceram Soc* 6:205–225
2. Weaver GQ (1982) Sintered high density boron carbide, US Patent No. 4,320,204
3. Lee H, Speyer RF (2003) Pressureless sintering of boron carbide. *J Am Ceram Soc* 86(9):1468–1473
4. Roy TK, Subramanian C, Suri AK (2006) Pressureless sintering of boron carbide. *Ceram Int* 32:227–233
5. Cho N (2006) Processing of boron carbide. Thesis, Georgia Institute of Technology
6. Jiao T, Li Y, Ramesh KT, Wereszczak AA (2004) High rate response and dynamic failure of structural ceramics. *Int J Appl Ceram Technol* 1(3):243–253
7. Luo H, Chen WW, Rajendran AM (2006) Dynamic compressive response of damaged and interlocked SiC-N ceramics. *J Am Ceram Soc* 89 (1):266–273

8. Paliwal B, Ramesh KT (2007) Effect of crack growth dynamics on the rate-sensitive behavior of hot-pressed boron carbide. *Scripta Mat* 57:481–484
9. Sano T, Chin ESC, Paliwal B, Chen MW (2009) Comparison of slip cast and hot pressed boron carbide. In: Bansal NP, Singh JP (eds) *Processing and properties of advanced ceramics and composites: ceramic transactions*, vol 203. Wiley, New Jersey, p 107
10. U.S. Department of Defense (1997) V50 ballistic test for armor, MJL-STD662, 18 Dec 1997
11. Woolsey P, Kokidko D, Mariano SA (1989) Alternative test methodology for ballistic performance ranking of armor ceramics. MTL TR 89-43, DTIC 1989
12. Dateraksa K, Sujirote K, McCuiston R, Atong D (2012) Ballistic performance of ceramic/S₂-glass composite armor. *J Magn Magn Mater* 22 (2):33–39
13. ASTM C1161-02c (2002) Standard test method for flexural strength of advanced ceramics at ambient temperature. *Annual book of ASTM standards*, vol 15.01. ASTM, West Conshohocken
14. ASTM C1326-96 (2003) Standard test method for Knoop indentation hardness of advanced ceramics. *Annual book of ASTM standards*, vol 15.01. ASTM, West Conshohocken
15. Swab JJ (2004) Recommendations for determining the hardness of armor ceramics. *Int J Appl Ceram Technol* 1(3):219–225
16. Vargas-Gonzalez L, Speyer RF, Campbell J (2010) Flexural strength, fracture toughness, and hardness of silicon carbide and boron carbide armor ceramics. *Int J Appl Ceram Technol* 7(5):643–651
17. Grady DE (1982) Local inertial effects in dynamic fragmentation. *J Appl Phys* 53(1):322–325
18. Lankford J, Blanchard CR (1991) Fragmentation of brittle materials at high rates of loading. *J Mater Sci* 26:3067–3072
19. Grady DE (2008) Fragment size distributions from the dynamic fragmentation of brittle solids. *Int J Imp Eng* 35:1557–1562
20. Zhua F, Molinari J-F, Ramesh KT (2005) A cohesive model based fragmentation analysis: effects of strain rate and defects distribution. *Int J Solids Struct* 42:5181–5207
21. Levy S, Molinari JF (2010) Dynamic fragmentation of ceramics, signature of defects and scaling of fragment sizes. *J Mech Phys Solids* 58:12–26
22. Keller AR, Zhou M (2003) Effect of microstructure on dynamic failure resistance of titanium diboride/alumina ceramics. *J Am Ceram Soc* 86 (3):449–457
23. Moynihan TJ, LaSalvia JC, Burkins MS (2002) Analysis of shatter gap phenomenon in a boron carbide/composite laminate armor system. In: *Proceedings of the 20th international symposium on ballistics*, Orlando, 23–27 Sept 2002

Dynamic Behavior of Materials, Volume 1
Proceedings of the 2013 Annual Conference on
Experimental and Applied Mechanics
Song, B.; Casem, D.; Kimberley, J. (Eds.)
2014, X, 496 p. 120 illus., Hardcover
ISBN: 978-3-319-00770-0